

PAPER

Conformable liquid metal printed epidermal electronics for smart physiological monitoring and simulation treatment

To cite this article: Xuelin Wang *et al* 2018 *J. Micromech. Microeng.* **28** 034003

View the [article online](#) for updates and enhancements.

Conformable liquid metal printed epidermal electronics for smart physiological monitoring and simulation treatment

Xuelin Wang¹, Yuxin Zhang¹, Rui Guo¹, Hongzhang Wang¹, Bo Yuan¹
and Jing Liu^{1,2} 

¹ Department of Biomedical Engineering, School of Medicine, Tsinghua University, Beijing 100084, People's Republic of China

² Technical Institute of Physics and Chemistry, Chinese Academy of Sciences, Beijing 100190, People's Republic of China

E-mail: jliubme@tsinghua.edu.cn

Received 24 August 2017, revised 2 January 2018

Accepted for publication 16 January 2018

Published 5 February 2018




CrossMark

Abstract

Conformable epidermal printed electronics enabled from gallium-based liquid metals (LMs), highly conductive and low-melting-point alloys, are proposed as the core to achieving immediate contact between skin surface and electrodes, which can avoid the skin deformation often caused by conventional rigid electrodes. When measuring signals, LMs can eliminate resonance problems with shorter time to reach steady state than Pt and gelled Pt electrodes. By comparing the contact resistance under different working conditions, it is demonstrated that both *ex vivo* and *in vivo* LM electrode–skin models have the virtues of direct and immediate contact with skin surface without the deformation encountered with conventional rigid electrodes. In addition, electrocardio electrodes composed of conformable LM printed epidermal electronics are adopted as smart devices to monitor electrocardiogram signals of rabbits. Furthermore, simulation treatment for smart defibrillation offers a feasible way to demonstrate the effect of liquid metal electrodes (LMEs) on the human body with less energy loss. The remarkable features of soft epidermal LMEs such as high conformability, good conductivity, better signal stability, and fine biocompatibility represent a critical step towards accurate medical monitoring and future smart treatments.

Keywords: liquid metal, epidermal electronics, physiological monitoring, simulation treatment

 Supplementary material for this article is available [online](#)

(Some figures may appear in colour only in the online journal)

1. Introduction

Noninvasion and precision for medical monitoring and treatment are the latest trends in the development of advanced health care devices. So far, conventional medical devices used in signal measurement or electrical stimulation treatment have been mainly equipped with rigid metallic electrodes such as cooper or platinum, which are generally placed directly on the skin [1–4]. However, due to the roughness of skin and irregular physiological profile of the human body [5], there often exist air gaps between rigid metallic electrodes and skin, inducing

bad Ohm contact which affects the measurement accuracy and even treatment effects [6, 7]. It has been shown that the poor coupling between metallic electrodes and skin may lead to low signal-to-noise ratio (SNR), which causes the degradation of signal performance when measuring physiological parameters [8]. In addition, low energy transfer efficiency between metallic electrodes and the target site caused by air gaps lead to energy accumulation and temperature rise on local skin surface, increasing the risk of skin injury [9]; this is especially reflected in equipment with high transient voltages such as defibrillators [10, 11].

To overcome the disadvantages of traditional rigid electrodes, researchers have tried to add pressure onto the electrodes to enhance electrode–skin contact [12]. However, the pressure applied may alter the electrical characteristics of the skin, causing measurement deviation. Conductive gels are also considered to promote the coupling performance. These gels could be smeared on the skin surface, filling the air gap between skin and electrode and enhancing the conductivity [13]. However, the resistance of the conductive gel itself cannot be ignored. Furthermore, the electrode cannot maintain good contact for long, which requires people to reconnect the electrodes, after monitoring, every 24 h.

Since flexible circuits can perfectly match the body curve and have excellent performance in electrophysiological and biochemical detection [14, 15], they are becoming more and more popular in wearable medical device fabrication for tasks such as body temperature measurement [16–18], blood flow measurement [17], and sweat analysis [19]. Due to their good electric coupling with skin, flexible circuits can achieve higher SNR, better security, and a more robust anti-motion effect [20]. Notably, existing flexible devices can fit the macrophysiological curve but cannot closely fit the microstructure on the skin surface.

With the capability of being printed directly on the skin, gallium-based liquid metals (LMs) show great potential for overcoming the technical challenges conventional rigid electrodes have faced [21–23]. Owing to the merits of non-toxicity and benign biocompatibility, LMs have made remarkable progress in bone cement [24], drug delivery nanomedicine [25], implantable devices [26], stretchable wireless sensors [27–29], electrical skin [30, 31], and wearable bioelectronics [32–35]. The favorable conformability [32, 33, 36] of LMs allow them to form a direct contact with the skin and even spontaneously fill the microstructure on the skin surface without external force [30, 31]. For instance, Yu *et al* have printed LM ink on a biological surface as a drawable electrocardiogram (ECG) electrode to demonstrate its conformability and attachment [31].

In this paper, a model is established to simulate the performance of the LM electrodes directly attached on the skin. *Ex vivo* and *in vivo* animal experiments of liquid metal electrodes (LMEs) are also taken to evaluate the electrode–skin coupling impedance in comparison to rigid electrodes. Additionally, stable ECG signals are detected to present the performance of physiological parameter monitoring. More importantly, a simulation treatment for smart defibrillation using these soft electrodes is done by analyzing the distribution of electric field and energy on the human body. The feasibility of highly conformable LM epidermal printed electronics meets the demands of medical applications, and provides a possible approach to future smart, accurate, and noninvasive physiological monitoring and treatment.

2. Materials and methods

2.1. Preparation of LM GaIn_{24.5}

The LM adopted as conformable epidermal bio-electrode was GaIn_{24.5} (EGaIn, melting point: 15.7 °C, conductivity:

$3.4 \times 10^6 \text{ S m}^{-1}$, polarization voltage dives to -0.73 V) [33]. Gallium and indium with purity above 99.99% were weighed according to the ratio of 75.5: 24.5. Liquid GaIn_{24.5} was obtained by mixing and stirring the prepared Gallium and Indium at 80 °C for 30 min. In order to avoid the adverse effects of the oxide layer on the LM surface, 10 ml NaOH solution (0.5 mol l^{-1}) was added, and the mixture was stirred for 1 min.

2.2. GaIn_{24.5} electrode–skin coupling model

To compare the differences between rigid Pt electrode, gelled Pt electrode, and LME, the contact impedances of Pt electrode–skin, gelled Pt electrode–skin, and GaIn_{24.5} electrode–skin in different frequencies from 1 to 10^5 Hz were measured on *in vivo* skin surface of 8 week BALB/c Nude mice by electrochemical workstation (CHI600E, Chenhua, China). In the Pt electrode–skin model, the Pt electrode was directly placed on the skin surface. In the gelled Pt electrode–skin model, the Pt electrode was placed on skin covered with conductive gel (ECG gel, Jinnuote). In the GaIn_{24.5} electrode–skin model, the Pt electrode was placed on skin covered with GaIn_{24.5}. When measuring contact impedances (figure S2), the working (green probe) and ground (black probe) electrodes are connected with the gelled Pt electrode or GaIn_{24.5} electrode (point A in figure 1(b)) via Pt wire; the reference (white probe) and auxiliary (red probe) electrodes are connected with skin surface (point B in figure 1(b)) via Pt wire. The epidermis of the nude mouse was very thin and the wire probe placed below the epidermis can be seen clearly. Therefore, both wire probes were visible and easily located. All data were measured at the same position to avoid individual difference.

To illustrate the effect of LME oxide skin on contact resistance, 0.1 mol l^{-1} HCl solution (Beijing Chemical Works), 0.1 mol l^{-1} NaCl solution (Sigma), and 0.1 mol l^{-1} NaOH solution (Sigma) were respectively treated on the *in vivo* skin surface of 8-week-old BALB/c Nude mice. A LM droplet was dripped on the mice skin first, and then the HCl, NaCl, or NaOH solution was dripped on the droplet. Four measuring electrodes were connected according to figure S2, and 5 min later, the contact resistances were measured by electrochemical workstation.

For the evaluation of contact situation, a CCD camera (JC2000D3, Shanghai) was used to capture the contact angles between the LM and skin surface. The contact angles of the LM droplet on the *ex vivo* skin surface of 8-week-old BALB/c Nude mice with different treatments (dry, wet (0.01 ml water on *ex vivo* skin surface), oil (0.01 ml oil on *ex vivo* skin surface)), was further measured and recorded (figure S1).

2.3. *In vivo* LME experiment

GaIn_{24.5} was prepared as described in section 2.1. Polydimethylsiloxane (PDMS) [39] was fabricated as a mixture of main and hardening agents (Dow Corning Sylgard 184, USA) with a mass ratio of 10:1. A plastic mold was first put in a plastic container, and then an electrode button was put on the mold. Then the PDMS mixture was poured into the container,

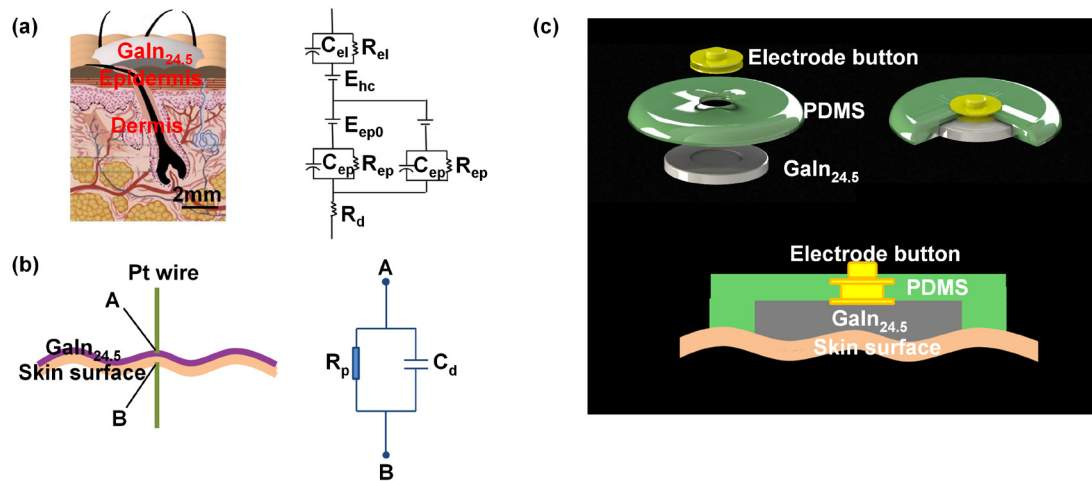


Figure 1. Schematic for skin electronics. (a) Structural diagram and electronic model of LM soft electrode-skin. (b) Simplified resistance capacitance parallel model of $\text{Galn}_{24.5}$ electrode-skin model. (c) 3D schematic diagram and its sectional drawing of LME.

surrounding the mold and the button. Then the container was put in a vacuum heater and heated to 70 °C until complete solidification. After this, the mold was removed; the device we finally acquired is shown in figure 1(c). The inside diameter of the LME model was 15 mm.

In vivo contact resistance under different working conditions (figure 3) was measured on adult male rabbits. $\text{Galn}_{24.5}$ was directly painted on shaved skin without other interface material, and a platinum electrode was implanted into the subcutaneous position relevant to LMEs. The backside, bosom, leg, and ear were chosen to measure the contact resistance by electrochemical workstation. Different concentrations of NaCl solution (0.5 mol l^{-1} , 1.0 mol l^{-1} , 1.5 mol l^{-1}) were applied to simulate the skin sweating process by smearing it on the skin. A thin layer of olive oil was painted on the skin to simulate skin oil secretion. Meanwhile, by changing the condition of the skin surface, external temperatures at 14 °C, 20 °C, and 27 °C were controlled to observe the influence on contact resistance.

When monitoring ECG signal via LMEs, a thin layer of $\text{Galn}_{24.5}$ was printed on the bosom of the rabbit by a spray printing method to make the electrode closely contact the skin as the first coating. In the printing process, the $\text{Galn}_{24.5}$ layer was printed by an airbrush (Meiji Piece Gun, Japan) under a specific mask as large as the LME surface [23]. The conformable LMEs, connected with the ECG monitor through three lead connections, were pasted on the printed $\text{Galn}_{24.5}$ layer to detect physiological signals (figures 3(e) and (f)). The animal study was approved by the Ethics Committee of Tsinghua University, Beijing, China under contract [SYXK(Jing)2009-0022].

2.4. Cytotoxicity and biocompatibility of $\text{Galn}_{24.5}$

The complete medium of human melanoma C8161 cells was made of 88% DMEM/F-12 (Gibco), 10% Certified Foetal Bovine Serum (Biological Industries), and 2% Penicillin-Streptomycin Solution (Corning). The complete medium of human epidermal HaCaT cells was made of 89% DMEM/High Glucose (HyClone), 10% Certified Foetal Bovine Serum

(Biological Industries), and 1% Penicillin-Streptomycin Solution (Corning). $\text{Galn}_{24.5}$ (0.2 ml) was immersed into the cell complete medium (10 ml) at different soak times (12, 24, 36, 48 h). Ion concentration of Gallium and Indium in cell culture medium at different soak times was detected by inductively coupled plasma mass spectrometry (Thermo X Series II, Thermo Fisher Scientific, Germany). The C8161 and HaCaT cells were cultured in the complete medium immersed by LM for 24 h and strained by Calcein AM/PI (LIVE/DEADTM Viability/Cytotoxicity Kit, Invitrogen) to detect the activity of the enzyme and the integrity of the plasma membrane. The living cells were green under fluorescence microscope excitation of 495 nm and the dead cells were red under fluorescence microscope excitation of 530 nm (Nikon ECLIPSE TS100). The C8161 and HaCaT cells were seeded on 96 well plates (cell concentration: $5 \times 10^4/\text{ml}$) with 100 $\mu\text{l}/\text{well}$ LM soaking medium. After culturing cells for 24 h, the original culture medium was removed, and 10 $\mu\text{l}/\text{well}$ CCK-8 (Cell Counting Kit-8, Dojindo) and 100 $\mu\text{l}/\text{well}$ fresh complete media were added. For 2 h culturing, the optical density was measured by the multifunctional enzyme marker (Varioskan Flash, Thermo Scientific) under excitation of 450 nm.

To test its biocompatibility, $\text{Galn}_{24.5}$ (0.1 ml/mouse) was injected underneath 8-week-old BALB/c Nude mice skin for different durations (0, 5, 10, 15 d) (figure S5), and then the skin was peeled off and stained with hematoxylin-eosin (HE) for histological analysis.

3. Results and discussion

3.1. The coupling impedance of $\text{Galn}_{24.5}$ electrode-skin model

Various models with different methods have been established to describe equivalent impedance of coupling between electrode and skin [7, 10, 37, 38]. In the rigid electrode-skin model, contact impedance between electrode and skin was affected by body motion because of the deformation of the skin [6]. In the rigid electrode-gel-skin model, the force caused by the contact between the electrode and skin was reduced by the gel

compared to the rigid electrode–skin model. Similarly, LMEs did not cause skin deformation, which could help reduce the impact of motion and mechanical force as well as maintain a stable electric potential E_{ep0} (figure 1(a)). The electrical resistivity of GaIn_{24.5} (44.1 $\mu\Omega\cdot\text{cm}$) was actually higher than common rigid electrodes such as copper (1.7 $\mu\Omega\cdot\text{cm}$), silver (1.6 $\mu\Omega\cdot\text{cm}$), and gold (2.2 $\mu\Omega\cdot\text{cm}$) [31]. However, the resistance could be ignored due to the close link between LME and skin. Besides, LMEs reduced the contact resistance between electrode and skin and therefore improved SNR of the measured signal. Furthermore, it diminished the impact of skin deformation on the transmission of electrical signals and thus improved the robustness. In figure 1(a), E_{hc} was half-cell potential; C_{el} and R_{el} were the total capacitance and resistance of the interface of electrode and electrolyte; C_{ep} and R_{ep} were the capacitance and resistance of the epidermis.

Due to the limitation of measurement, the whole electrode–skin model was simplified as a parallel model consisting of resistance R_p and capacitance C_d (figure 1(b)). Consequently, the overall impedance could be characterized as

$$Z = \frac{1}{Y} = \frac{R_p}{1 + j\omega C_d R_p} = \frac{R_p (1 - j\omega C_d R_p)}{1 + (\omega C_d R_p)^2} \quad (1)$$

$$Z = \frac{R_p}{1 + (\omega C_d R_p)^2} - j \frac{\omega C_d R_p^2}{1 + (\omega C_d R_p)^2}. \quad (2)$$

Here, Z is the impedance (Z' being the real part; Z'' being the imaginary part), Y is the admittance (the reciprocal of Z), ω is the angular frequency (unit: rad s^{-1}), and j is the imaginary number. The real part Z' and imaginary part Z'' of the overall impedance measured from frequency response analysis could be further described as follows:

$$Z' = \frac{R_p}{1 + (\omega C_d R_p)^2} \quad (3)$$

$$Z'' = \frac{\omega C_d R_p^2}{1 + (\omega C_d R_p)^2}. \quad (4)$$

As a result, the resistance R_p and capacitance C_d could be calculated by

$$R_p = Z' \left(1 + \left(\frac{Z''}{Z'} \right)^2 \right) \quad (5)$$

$$C_d = \frac{Z''}{Z' \omega R_p}. \quad (6)$$

In figures 2(a) and (b), the impedance variation tendency under different frequencies had obvious distinction among Pt electrode–skin, gelled Pt electrode–skin, and GaIn_{24.5} electrode–skin models. Among these three types of electrodes, the gelled Pt electrode–skin model had the least resistance, while the Pt electrode–skin model had the most resistance. At the frequency of 10 Hz, the EGaIn resistance was $3.04 \times 10^4 \Omega$, the Pt resistance was $6.32 \times 10^4 \Omega$ (2.08 times to EGaIn), and the gelled-Pt resistance was $1.60 \times 10^4 \Omega$ (0.53 times to EGaIn). The Pt electrode–skin model had the least

capacitance, and the capacitance of the GaIn_{24.5} electrode–skin model was lower than that of the gelled Pt electrode–skin model within the whole measured frequency range. At frequency of 10 Hz, the EGaIn capacitance was $5.75 \times 10^{-7} \text{ F}$, the Pt capacitance was $2.85 \times 10^{-7} \text{ F}$ (0.49 times to EGaIn), and the gelled-Pt capacitance was $2.20 \times 10^{-6} \text{ F}$ (3.83 times to EGaIn). The product of R_p and C_d is the time constant of the resistance–capacitance circuit. Taking the frequency of 10 Hz for instance, the $R_p \cdot C_d$ of EGaIn was $1.748 \times 10^{-2} \text{ s}$, the $R_p \cdot C_d$ of Pt was $1.8012 \times 10^{-2} \text{ s}$, and the $R_p \cdot C_d$ of gelled Pt was $3.52 \times 10^{-2} \text{ s}$. From this analysis, the time constant of the gelled-Pt electrode was the largest and the charging time that gelled-Pt electrode required to reach the steady state was the longest, which hindered the stability of signal measurement. Due to its maximal capacitance, the gelled Pt electrode–skin model caused more oscillation in the circuit than GaIn_{24.5} or Pt electrode–skin model, even though its resistance had the lowest value.

Figures 2(c) and (d) demonstrate that the GaIn_{24.5} electrode–skin model had the maximum resistance and the minimum capacitance under HCl treatment. NaCl treatment produced the largest capacitance and NaOH treatment produced the smallest resistance. 0.1 mol l⁻¹ HCl and 0.1 mol l⁻¹ NaOH solutions could totally dissolve the thin oxide skin of the LM [40, 41]. By comparing the resistance and capacitance resulting from NaCl and NaOH treating, we determined there was a distinguishing relationship between contact impedances and the oxide skin of the LM. Oxide skin increased the contact impedance between EGaIn and skin. EGaIn/HCl resistance had the maximum value because of the volatility of HCl. Its volatility led to fewer ions between LM and skin than those treated by NaOH solution, which made EGaIn/HCl resistance greater than that of EGaIn/NaOH. According to the formula $C = \varepsilon \cdot \varepsilon_0 \cdot S/d$, the ε of EGaIn was smaller than that of NaOH or NaCl solution (some of HCl volatilized, which reduced the concentration of the HCl solution). Therefore, EGaIn/HCl had the least capacitance. On the whole, the oxide layer of LM droplet on *ex vivo* BALB/c Nude mouse skin increased the contact impedances.

3.2. *In vivo* physiological monitoring with GaIn_{24.5} LME

Figure 3 presents *in vivo* GaIn_{24.5} electrode–skin contact resistance under different working conditions for the purpose of evaluating the conformability of the GaIn_{24.5} electrode. Figure 3(a) demonstrates that the contact resistance of dry skin was higher than that with NaCl solution (0.5, 1.0, 1.5 mol l⁻¹) under low frequency. However, the treatment on skin by different concentrations of NaCl solution brought about the same contact resistance. The contact resistance of oily skin–GaIn_{24.5} was higher than that of dry skin–GaIn_{24.5} and normal saline skin–GaIn_{24.5}, and normal saline skin–GaIn_{24.5} had the lowest contact resistance (figure 3(b)). Figure 3(c) demonstrates that the contact resistance of skin–GaIn_{24.5} varied under different room temperatures (14, 20, 27 °C). The contact resistance was the largest at 14 °C, was slightly lower at 20 °C, and was the lowest at 27 °C. Figure 3(d) illustrates the contact resistance measurement under different positions. The

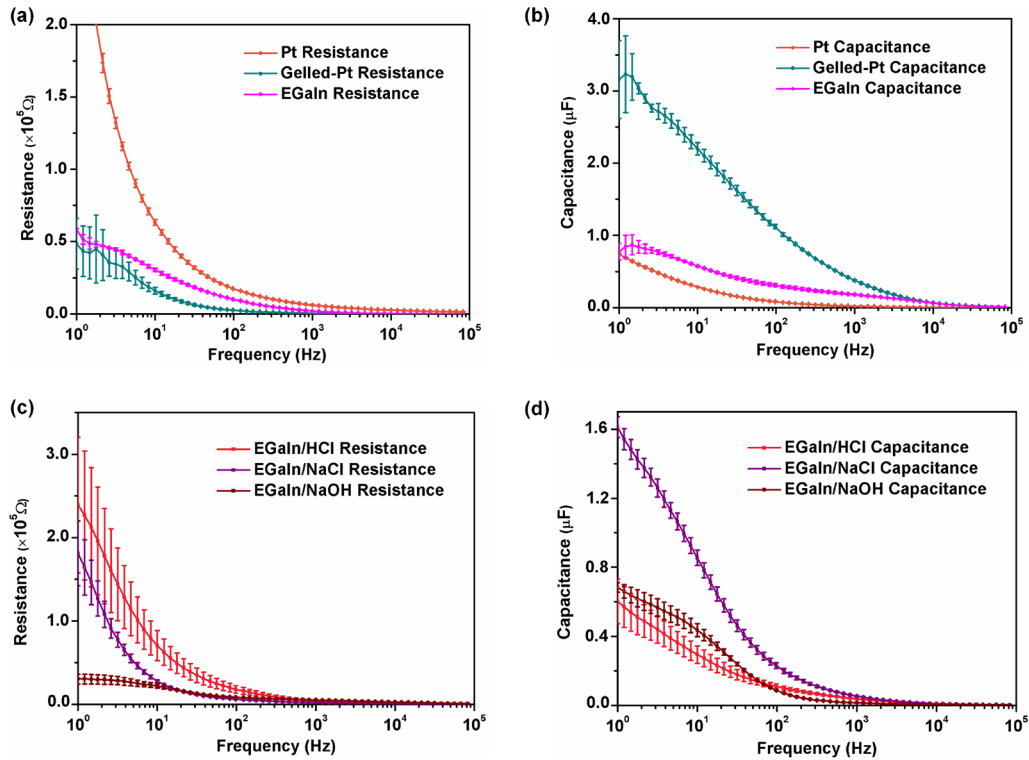


Figure 2. Experimental data. (a) and (b) Curves of resistance and capacitance of GaIn_{24.5} electrode–skin, Pt electrode–skin, and gelled Pt electrode–skin varying with frequency from 1 to 10⁵ Hz. ‘Pt Resistance’ refers to the resistance of Pt electrode–skin; ‘Gelled-Pt Resistance’ refers to the resistance of gelled Pt electrode–skin; ‘EGaIn Resistance’ refers to the resistance of GaIn_{24.5} electrode–skin; ‘Pt Capacitance’ refers to the capacitance of Pt electrode–skin; ‘Gelled-Pt Capacitance’ refers to the capacitance of gelled Pt electrode–skin; ‘EGaIn Capacitance’ refers to the capacitance of GaIn_{24.5} electrode–skin. (c) and (d) Curves of resistance and capacitance of GaIn_{24.5} electrode–skin under different skin surface treatments (0.1 mol l⁻¹ HCl, 0.1 mol l⁻¹ NaCl, 0.1 mol l⁻¹ NaOH).

ear was the largest, followed by backside and bosom, and the leg was the least.

By measuring the contact resistance between a GaIn_{24.5} bioelectrode and skin surface under different working conditions, we evaluated the conformability of LMEs. The inset of figure 3(a) revealed that positive and negative ions in NaCl solution enhanced the ion transfer and reduced the resistance. Actually, because the ions in 0.5 mol l⁻¹ NaCl solution are enough for current transfer, increasing the solution concentration could not reduce the contact resistance obviously. Contact resistance was increased with oily skin and the curve fluctuation was quite large in the low-frequency region, which indicated that the contact resistance was changed largely and signal anti-interference ability was weakened (figure 3(b)).

Rabbits are warm-blooded animals. When external temperature was far lower than the rabbit body temperature, gooseflesh would occur on the rabbit skin surface to adjust the skin temperature. Gooseflesh reduces the smoothness of the skin so that the contact resistance increased when external temperature was decreased (figure 3(c)). Meanwhile, the reduced temperature also transformed LM from liquid to solid, which reduced the conformability of LMEs. Therefore, LMEs had a relatively narrow temperature range for application and should be further tested by LMs with a lower melting point than GaIn alloy, such as Ga–In–Sn (Ga_{62.5}In_{21.5}Sn₁₆,

melting point: 11 °C) or Ga–In–Sn–Zn (Ga₆₁In₂₅Sn₁₃Zn₁, melting point: 7 °C) [25].

At different parts of the rabbit, the body profile had different shapes and contact resistance varied greatly (figure 3(d)). When measuring the contact resistance of the ear, it had not been shaved and its resistance was the greatest. With regard to the spine’s presence on the backside, its surface was not flat and its contact resistance was the second greatest. Smooth surfaces at the bosom and leg had been chosen, but more subcutaneous fat in the chest leads to larger contact resistance than in the leg. Hence, the contact resistances were similar in different working conditions at high frequency (up to 10 Hz) that were in the frequency range for ECG, electroencephalogram, pulse wave, and electromyographic detection.

The LMEs were applied to ECG monitoring. By comparing ECG signals measured by LMEs and Ag/AgCl electrodes, we found similar stable ECG signals between LMEs and traditional Ag/AgCl electrodes. The ECG signal measured by LMEs had uniform variation comparing to Ag/AgCl electrodes with undulating signal (figures 3(e) and (f)). The variation of peak-to-peak voltage detected by Ag/AgCl electrodes (32.45 μV) was 3.15 times larger than that monitored by LMEs (10.31 μV). As a result, the maximal ECG signal value measured by Ag/AgCl electrodes changed more dramatically than that of LMEs, which meant LMEs presented better signal stability and certain reduction of noise.

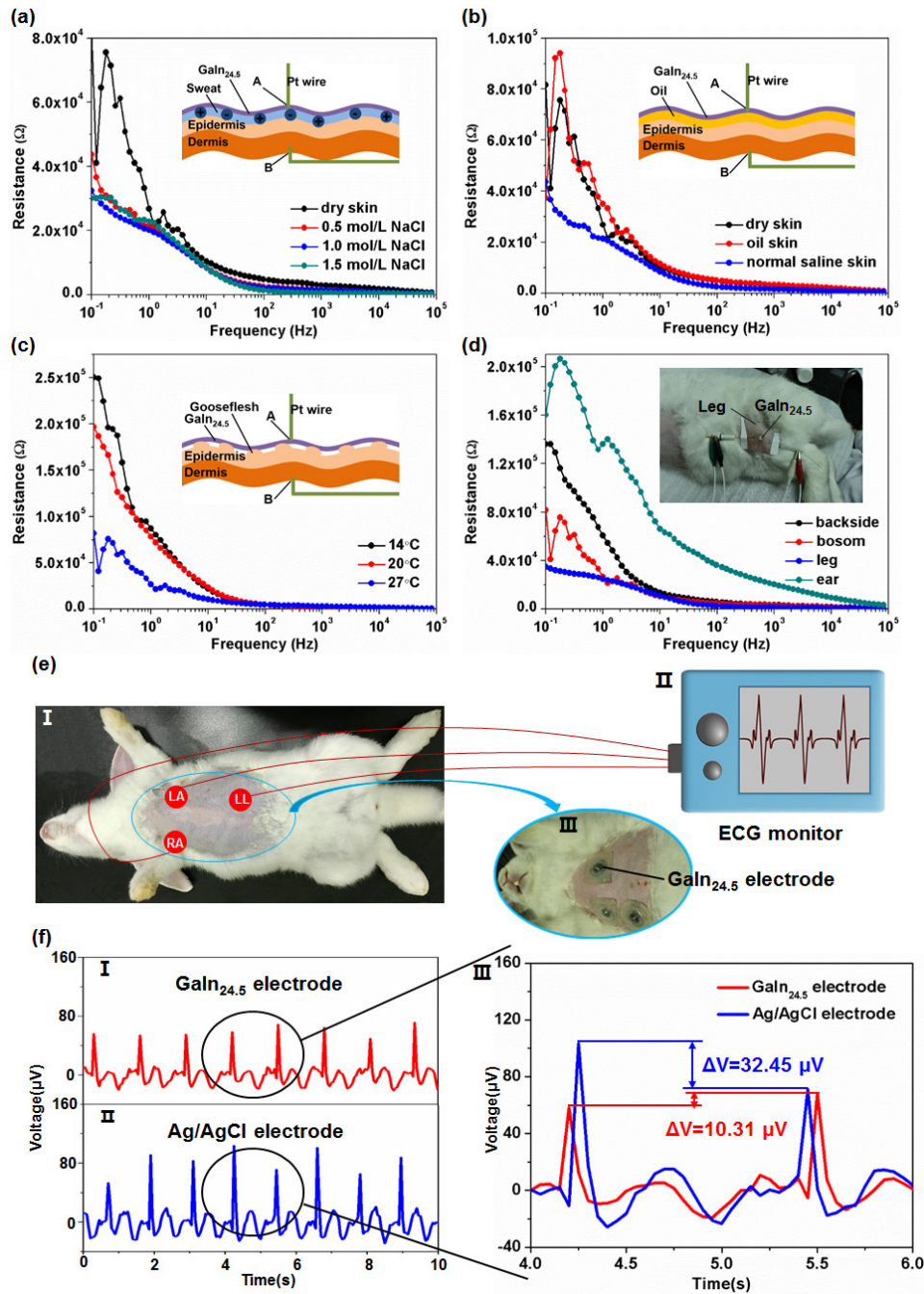


Figure 3. Contact resistance of GaIn_{24.5} under different working conditions and the ECG signal measurement of the rabbit. (a) Contact resistance under different NaCl concentrations. (b) Contact resistance under dry, oily, and normal saline skin. (c) Contact resistance under different temperatures. (d) Contact resistance under different measuring positions. (e) Connection of LMEs and ECG monitor: (I) sketch of three ECG leads on rabbit chest, (II) ECG monitor measuring ECG signal, (III) LMEs on rabbit chest. (f) ECG signals respectively measured by LMEs and Ag/AgCl electrodes: (I) ECG signal measured by LMEs, (II) ECG signal measured by Ag/AgCl electrodes, (III) ECG signal comparison between LMEs and Ag/AgCl electrodes from 4 to 6 s.

3.3. Simulation smart defibrillation treatment using conformable LMEs

To evaluate the treatment of smart defibrillation using LMEs, physical field simulation was carried out to examine the conductivity of LM electrode–skin (see supplementary information (stacks.iop.org/JMM/28/034003/mmedia) for finite element simulation details) [42, 43]. The LME was closely attached to the skin, and hence the electric potential

distribution along the normal direction of skin varied evenly (figure 4(b)). In comparison, rigid electrodes only contacted convex skin surface and the electric potential distribution in the concave was small (figure 4(a)). The electric field distribution of flexible electrodes was more uniform compared to that of rigid electrodes (figures 4(a) and (b)). Since the directions of current and electric field were always consistent, flexible electrodes were able to generate effects uniformly regardless of the direction of current. In contrast, the air gap between

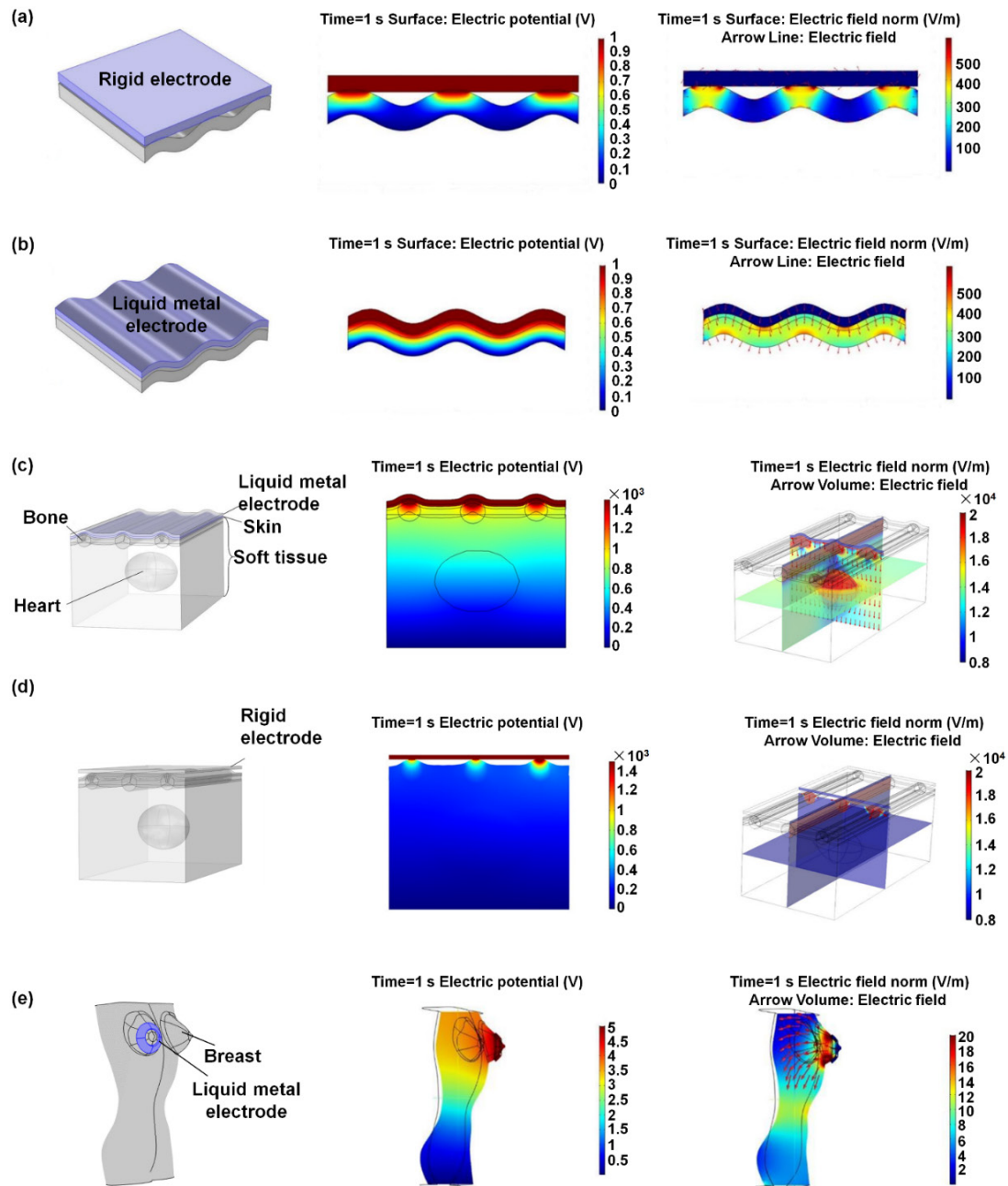


Figure 4. Physical field simulation of rigid and conformable LM bioelectrodes on skin surface and human body models, respectively. (a) Electric potential distribution and electric field distribution of skin when applying voltage in rigid electrode–skin model (purple area is copper electrode). (b) Electric potential distribution and electric field distribution of skin when applying voltage in LM electrode–skin model (purple area is LME). (c) Defibrillation model of flexible LME covering human chest, and electric potential and electric field distribution of physical field simulation in flexible LME model. (d) Defibrillation model of conventional rigid electrode covering human chest, and electric potential and electric field distribution of physical field simulation in rigid electrode model. (e) Model of ring LME covering female breast, and electric potential and electric field distribution of physical field simulation in ring LME model (purple area is LME).

rigid electrode and skin resulted in high impedance, which might generate heat that could damage the skin (bright spot in figure S4).

Further, based on the electrode–skin models shown formerly, figures 4(c) and (d) exhibit the models of flexible LME and conventional rigid electrode covered on the chest of the human body to simulate the treatment for defibrillation via electrical effect. The simplified chest geometric model was divided into five parts, including electrode, skin, bone,

tissue, and heart. As shown in figure 4(c), LME closely fitted the skin surface, but with the rigid electrode, air remained in the gap (figure 4(d)). The electrical parameters of the material were shown in table SI. In order to control the variables and compare the difference between flexible and rigid electrodes, we chose LM GaIn_{2.5} for the flexible electrodes and copper for the rigid one. The upper surface of the LME was applied with a voltage input to simulate the process of defibrillation more realistically. Through the analysis of electrical

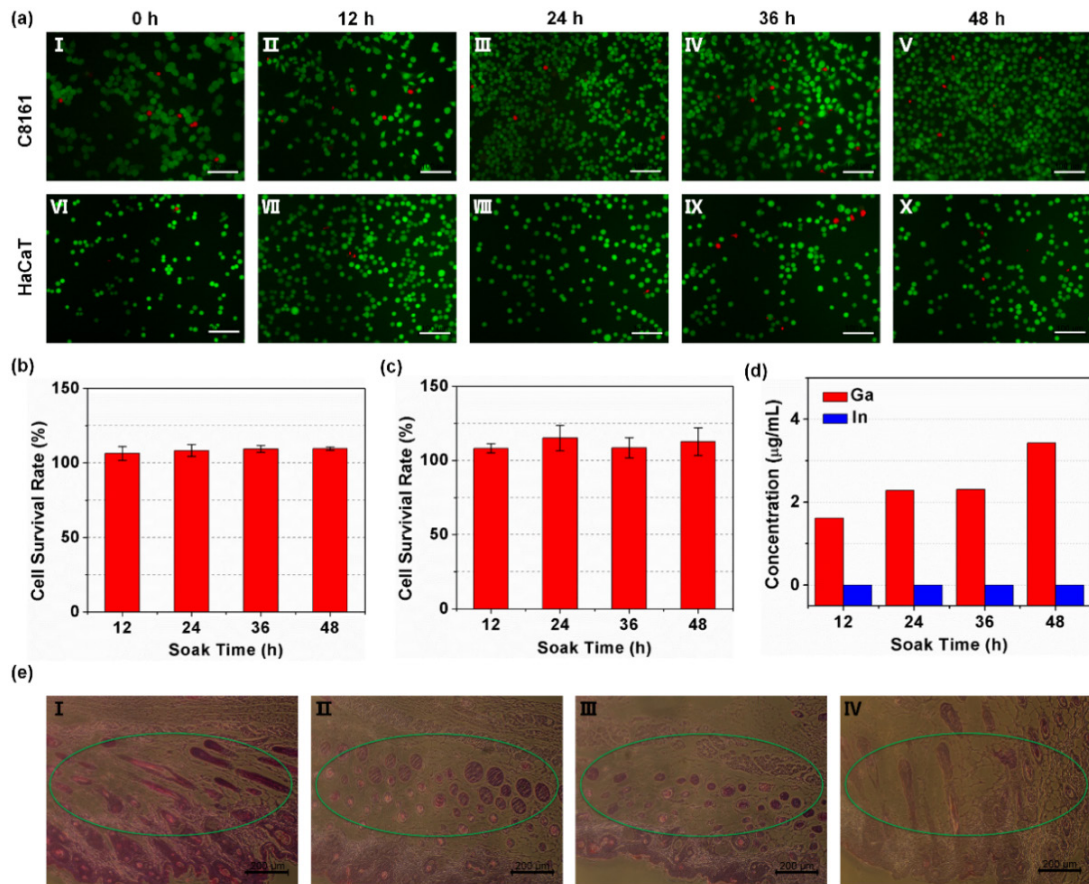


Figure 5. Cytotoxicity and biocompatibility of GaIn_{24.5}. (a) Observations of live and dead cells of human melanoma C8161 cells and human epidermal HaCaT cells under fluorescence microscope with cell culture medium immersed in GaIn_{24.5} (soak times: 12, 24, 36, 48 h); scale bars: 100 μm . (b) Survival rate of human melanoma C8161 cells by CCK-8 assay with cell culture medium immersed in GaIn_{24.5} (soak times: 12, 24, 36, 48 h). (c) Survival rate of human epidermal HaCaT cells by CCK-8 assay with cell culture medium immersed in GaIn_{24.5} (soak times: 12, 24, 36, 48 h). (d) Ion concentration in cell culture medium at different soak times (12, 24, 36, 48 h) immersed in GaIn_{24.5}. (e) Skin biopsies with 0.1 ml GaIn_{24.5} injected underneath BALB/c Nude mice skin for different durations (0, 5, 10, 15 d); scale bars: 200 μm .

potential distribution and electric field distribution, the flexible LME needed less energy input to realize the same current distribution.

Defibrillation treatment models (figures 4(c) and (d)) revealed that bone barrier led to uneven body profile, making it hard for the rigid electrode to pass enough current to the heart, especially when the patient was thin. However, the highly conformable bioelectrode had good contact with skin, decreasing the surface resistance and avoiding heat accumulation and skin ambustion. When smeared with the conductive paste, the gap between the electrode and skin would be filled. The conductivity of the conductive paste was $1\text{--}20\text{ S m}^{-1}$ and the GaIn_{24.5} electrode was $3.76 \times 10^6\text{ S m}^{-1}$. Therefore, LME could reduce the energy attenuation and more energy could be transmitted to the heart compared to that transmitted with conventional conductive paste.

Additionally, to verify the conformability of LMEs, a ring LME model was built on a female breast (figure 4(e)). Owing to the fine structure on the contact of breast and electrodes, there was a high mesh division density as shown in figure S3(c). Mesh division density at electrode–breast

junction region was the highest, with a minimal grid density of 0.1 mm. In the ring electrode model, the human body was assumed as being homogeneous soft tissue. Uniform electric potential and electric field distribution were obtained by the ring electrode tightly fitting the skin curve, highlighting the merits of suitable flexible electrodes. To sum up, all LMEs employed in measurement or treatment achieved good contact with the human body.

3.4. Cytotoxicity and biocompatibility of GaIn_{24.5}

Human melanoma C8161 cells and human epidermal HaCaT cells were applied to detect the cytotoxicity of LM GaIn_{24.5}. Figure 5(d) shows the ion concentration of gallium and indium in cell culture medium immersed in GaIn_{24.5} for different soak times (12, 24, 36, 48 h). Indium was stable and not detected even after 48 h immersion [44]. The C8161 cells and the HaCaT cells cultured in the complete medium immersed by LM were mostly alive (figure 5(a); green, live; red, dead). The cell survival rate of the C8161 and HaCaT cells (figures 5(b) and (c)) was higher than 100% with different soak times,

which demonstrated the nontoxicity of complete medium immersed in GaIn_{24.5}.

In addition, GaIn_{24.5} was painted on the skin of BALB/c Nude mouse for 30 min and totally cleaned up with 75% alcohol. No inflammation was observed, indicating that LM did not cause skin irritation and did not influence the breathable function of the skin (movie S1, figure S6). Furthermore, the HE slices of skin biopsies (figure 5(e), green circle; circular follicles show inflammatory reaction) indicate an inflammatory reaction at 5 d that was weakened at 10 d and disappeared at 15 d, showing its good biocompatibility.

4. Conclusion

In summary, conformable LMEs showed low contact resistance, low noise signal acquisition, little energy diminution, and fine biocompatibility. Its good contact with skin was proven by favorable electrical conduction. Due to its conformability, GaIn_{24.5} can not only adapt well to the human body profile, but can also fit the microstructure of the skin surface without causing evident force, avoiding both deformation and electrical property change of the electrode–skin interface. Particularly when comparing the LM electrode–skin model with rigid electrode–skin and rigid electrode–gel–skin models, LME offered optimal coupling impedance. In addition, the contact resistance of the LM GaIn_{24.5} electrode–skin model measured under different working conditions such as sweat or oil secretion, different temperature, and different body profiles, illustrated its adaptability in different environments. ECG signal monitored by LMEs had less noise and better signal stability than that monitored by Ag/AgCl electrodes. More importantly, simulation treatment for smart defibrillation of thoracic model electric field distribution achieved precise therapy by establishing the theory of cardiac defibrillation via FEM (finite element method) simulation. Conformable LMEs showed the capability of displaying more uniform electric potential and electric field distribution with less energy loss compared to conventional rigid electrodes. Besides, fluorescence imaging of live/dead cells and the survival rate of C8161 and HaCaT cells indicated its nontoxicity, and the weakening of inflammation showed its excellent biocompatibility. Therefore, flexible LM electronics offer an excellent way to realize direct and immediate electrode–skin contact, with high conformability and good conductivity, to improve stability and precision in physiological monitoring and disease treatment.

Except for the contact impedance of the electrode–skin model, more validations are needed to examine the capability of LME to transmit electrical physiological signals under different working conditions. Apart from the simplified simulation models with uniform structure, some more realistic simulations with real human body size, structure, and organization type may also need to be considered to improve the treatment effects for defibrillation. For example, it is envisioned that the human body model established by CT (computer tomography) and MRI (magnetic resonance imaging) images can be adopted in the simulation, which

would be very helpful to plan formulation for personalized accurate treatment according to each specific patient. Overall, the presently established, highly conformable LM printed epidermal electronics offer an extraordinary solution for physiological signal monitoring, human disease treatment, and overcoming medical challenges in the near future.

Acknowledgments

This work is partially supported by the NSFC Key Project under Grant 91748206, the Ministry of Higher Education Equipment Development Fund, Dean's Research Funding, and the Frontier Project of the Chinese Academy of Sciences.

ORCID iDs

Jing Liu  <https://orcid.org/0000-0002-0844-5296>

References

- [1] Shimizu H 2007 *Shimizu's Textbook of Dermatology* 1st edn (Sapporo City: Nakayama Shoten, Hokkaido University Press) ch 1
- [2] Kletenik Y B and Aleksandrova T P 1997 Submicron regeneration of the working surface of indicator electrodes: regeneration of metal electrodes *J. Anal. Chem.* **52** 680–2
- [3] Lehw G and Nicolelis M A L 2008 State-of-the-art microwire array design for chronic neural recordings in behaving animals *Methods for Neural Ensemble Recordings* 2nd edn (Boca Raton, FL: CRC Press) pp 361–71
- [4] Lee H, Kim H B, Im T G, Jeong J I and Ahn S 2003 Characterization of platinum electrode using unbalanced magnetic field sputter for implantable biomedical applications *30th Int. Conf. on Plasma Science*, p 291
- [5] Wu F, Wang L, Zou J, Huang X and Yuan X 2012 Clinical features, mutation of the GNAS1 and pathogenesis of progressive osseous heteroplasia *Chin. J. Pediatrics* **50** 10–4
- [6] Cömert A, Honkala M and Hyttinen J 2013 Effect of pressure and padding on motion artifact of textile electrodes *Biomed. Eng. Online* **12** 26
- [7] He L, Lin D, Wang Y, Xiao Y and Che J 2011 Electroactive SWNT/PEGDA hybrid hydrogel coating for bio-electrode interface *Colloids Surf. B* **87** 273–9
- [8] Bera S C, Chattopadhyay S and Chakraborty B 2004 An experimental analysis of the non-linear behaviour of a bio-electrode polarisation impedance with excitation frequency *Measurement* **35** 363–70
- [9] Plam U, Keeser D, Schiller C, Fintescu Z, Nitsche M, Reisinger E and Padberg F 2008 Skin lesions after treatment with transcranial direct current stimulation (tDCS) *Brain Stimul.* **1** 386–7
- [10] Esibov A, Chapman F W, Melnick S B, Sullivan J L and Walcott G P 2015 Minor variations in electrode pad placement impact defibrillation success *Prehosp. Emerg. Care* **20** 292–8
- [11] Killingsworth C R, Melnick S B, Litovsky S H, Ideker R E and Walcott G P 2013 Evaluation of acute cardiac and chest wall damage after shocks with a subcutaneous implantable cardioverter defibrillator in swine *Pacing Clin. Electrophysiol.* **36** 1265–72
- [12] Martins A C, Moreira A, Machado A V, Vaz F, Fonseca C and Nóbrega J M 2015 Development of polymer wicks for

- the fabrication of bio-medical sensors *Mater. Sci. Eng. C* **49** 356–63
- [13] Xu S, Dai M, Xu C, Chen C, Tang M, Shi X and Dong X 2011 Performance evaluation of five types of Ag/AgCl bio-electrodes for cerebral electrical impedance tomography *Ann. Biomed. Eng.* **39** 2059–67
- [14] Abellán-Llobregat A, Jeerapan I, Bandodkar A, Wang J and Morallón E 2017 A stretchable and screen-printed electrochemical sensor for glucose determination in human perspiration *Biosens. Bioelectron.* **91** 885–91
- [15] Mishra R K, Hubble L J, Martín A, Kumar R and Wang J 2017 Wearable flexible and stretchable glove biosensor for on-site detection of organophosphorus chemical threats *ACS Sensors* **2** 553–61
- [16] Zhang Y, Webb R C, Luo H, Xue Y, Kurniawan J, Cho N H, Krishnan S, Li Y, Huang Y and Rogers J A 2016 Theoretical and experimental studies of epidermal heat flux sensors for measurements of core body temperature *Adv. Healthc. Mater.* **5** 119–27
- [17] Webb R C, Ma Y, Krishnan S, Li Y, Yoon S, Guo X, Feng X and Rogers J A 2015 Epidermal devices for noninvasive, precise, and continuous mapping of macrovascular and microvascular blood flow *Sci. Adv.* **1** e1500701
- [18] Gao L, Zhang Y, Malyarchuk V, Jia L, Jang K-I, Webb R C and Rogers J A 2014 Epidermal photonic devices for quantitative imaging of temperature and thermal transport characteristics of the skin *Nat. Commun.* **5** 4938
- [19] Huang X, Liu Y, Chen K, Shin W-J, Lu C-J, Kong G-W and Rogers J A 2014 Stretchable, wireless sensors and functional substrates for epidermal characterization of sweat *Small* **10** 3083–90
- [20] Neuman M R 1997 Biopotential electrodes *Medical Instrumentation: Application and Design* 3rd edn, ed J G Webster (New York: Wiley) pp 183–232
- [21] Guo C, Yu Y and Liu J 2014 Rapidly patterning conductive components on skin substrates as physiological testing devices via liquid metal spraying and pre-designed mask *J. Mater. Chem. B* **2** 5739–45
- [22] Li J, Guo C, Wang Z, Gao K, Shi X and Liu J 2016 Electrical stimulation towards melanoma therapy via liquid metal printed electronics on skin *Clin. Trans. Med.* **5** 21
- [23] Zhang Q, Zheng Y and Liu J 2012 Direct writing of electronics based on alloy and metal (DREAM) ink: a newly emerging area and its impact on energy, environment and health sciences *Front. Energy* **6** 311–40
- [24] Yi L, Jin C, Wang L and Liu J 2014 Liquid–solid phase transition alloy as reversible and rapid molding bone cement *Biomaterials* **35** 9789–801
- [25] Lu Y, Hu Q, Lin Y, Dickey M D and Gu Z 2015 Transformable liquid-metal nanomedicine *Nat. Commun.* **6** 10066
- [26] Jin C, Zhang J, Li X, Yang X, Li J and Liu J 2013 Injectable 3D fabrication of medical electronics at the target biological tissues *Sci. Rep.* **3** 3442
- [27] Jeong S H, Hjort K and Wu Z 2015 Tape transfer atomization patterning of liquid alloys for microfluidic stretchable wireless power transfer *Sci. Rep.* **5** 8419
- [28] Cheng S and Wu Z 2012 Microfluidic electronics *Lab Chip* **12** 2782–91
- [29] Cheng S and Wu Z 2011 A microfluidic, reversibly stretchable, large-area wireless strain sensor *Adv. Funct. Mater.* **21** 2282–90
- [30] Jeong S H, Hagman A, Hjort K, Jobs M, Sundqvist J and Wu Z 2012 Liquid alloy printing of microfluidic stretchable electronics *Lab Chip* **12** 4657–64
- [31] Yu Y, Zhang J and Liu J 2013 Biomedical implementation of liquid metal ink as drawable ECG electrode and skin circuit *PLoS One* **8** e58771
- [32] Wang Q, Yu Y, Yang J and Liu J 2015 Fast fabrication of flexible functional circuits based on liquid metal dual—trans printing *Adv. Mater.* **27** 7109–16
- [33] Matsuzaki R and Tabayashi K 2015 Highly stretchable, global, and distributed local strain sensing line using GaInSn electrodes for wearable electronics *Adv. Funct. Mater.* **25** 3806–13
- [34] Krupenkin T and Taylor J A 2011 Reverse electrowetting as a new approach to high-power energy harvesting *Nat. Commun.* **2** 73–86
- [35] Wang X L and Liu J 2016 Recent advancements in liquid metal flexible printed electronics: properties, technologies, and applications *Micromachines* **7** 206
- [36] Boley J W, White E L, Chiu G T-C and Kramer R K 2014 Direct writing of gallium–indium alloy for stretchable electronics *Adv. Funct. Mater.* **24** 3501–7
- [37] Lu T, Finkenauer L, Wissman J and Majidi C 2014 Rapid prototyping for soft—matter electronics *Adv. Funct. Mater.* **24** 3351–6
- [38] Goran L, Zoran V, Mihailo L, Jovana S-K and Đuro K 2014 Modeling of bioimpedance for human skin based on fractional distributed-order modified cole model *FME Trans.* **42** 74–81
- [39] Luna J L V, Krenn M, Ramirez J A C and Mayr W 2015 Dynamic impedance model of the skin-electrode interface for transcutaneous electrical stimulation *PLoS One* **10** e0130368
- [40] Bilodeau R A, Zemlyanov D Y and Kramer R K 2017 Liquid metal switches for environmentally responsive electronics *Adv. Mater. Interfaces* **4** 1600913
- [41] Carle F, Bai K, Casara J, Vanderlick K and Brown E 2016 Development of magnetic liquid metal suspensions for magnetohydrodynamics (arXiv:1512.02575v3)
- [42] Wang P, Liu J, Liu Z and Chen Y 2017 Experiment and simulation of natural convection heat transfer of transformer oil under electric field *Int. J. Heat Mass Transf.* **115** 441–52
- [43] Sel D, Mazeris S, Teissie J and Miklavcic D 2003 Finite-element modeling of needle electrodes in tissue from the perspective of frequent model computation *IEEE Trans. Biomed. Eng.* **50** 11
- [44] <http://datasheets.scbt.com/sc-257605.pdf>